J. Deur, B. Škugor, W. Chen, Y. Zhang, E. Dai, "Energy-efficient Straight-line Driving Torque Vectoring for Electric Vehicles with Multiple Motors Equipped with Disconnect Clutches", 18th Conference on Sustainable Development of Energy, Water, and Environment Systems (SDEWES), accepted, pp. 1-15, Sep. 2023.

Energy-efficient Straight-line Driving Torque Vectoring for Electric Vehicles with Multiple Motors Equipped with Disconnect Clutches

Joško Deur[1)], Branimir Škugor[1)*], Weitian Chen[2)], Yijing Zhang[2)], Edward Dai[2)]

[1)]University of Zagreb, Faculty of Mechanical Engineering and Naval Architecture, Zagreb, Croatia

[2)]Ford Research and Advanced Engineering, Dearborn, MI, USA

[*]Corresponding author; e–mail: branimir.skugor@fsb.hr

ABSTRACT

Battery electric vehicles with multiple motors are characterized by actuator redundancy, which calls for application of instantaneously optimized distribution of motor/wheel torques, thus minimizing the energy consumption, i.e., maximizing the vehicle range. If the e-motors are equipped with disconnect clutches, the energy saving potential becomes even higher due to the avoidance of drag of inactive e-motors. However, in this case optimization through time and predictive control techniques should be used to provide globally minimal energy consumption. To, this end, the paper proposes the following modeling, optimization, and control methods for straight-line driving mode: (i) a dynamic backward-looking model of electric vehicle propelled by disconnect clutch-equipped four wheel motors, which takes into account the clutch synchronization-related drivetrain transient loss; (ii) globally optimal, dynamic programming (DP)-based off-line optimization of e-motor torque and clutch state control trajectories, (iii) a parameter-optimized rule-based (RB) torque vectoring control strategy, and (iv) a model predictive torque vectoring control (MPC) strategy. The control strategies are verified by simulation for various certification driving cycles, and the results are compared with the DP-optimal benchmark for different values of a user-defined weighting coefficient, which penalizes frequent clutch disconnects for improved durability. The DP optimization results reveal that the energy consumption reduction achieved through the disconnect clutch functionality is up to 7%, on top of up to 5% reduction achieved by torque distribution itself. The RB and MPC control strategies approach the DP energy consumption benchmark within the margin of 1.3% and 0.6%, respectively.

KEYWORDS

Electric vehicles, torque vectoring, energy efficiency, modeling, optimization, dynamic programming, rule-based control, model predictive control, straight-line driving

1. INTRODUCTION

Configuring the battery electric vehicles with multiple e-motors is mainly motivated by achieving significantly enhanced vehicle dynamics performance. For instance, using two motors, one on each side of a single axle (an active differential), provides generation of active yaw torque for safer, better damped, and more agile lateral vehicle dynamics control [1]. Alternatively, using two motors to drive each axle via mechanical differentials leads to an all-wheel drive (AWD) configuration characterized by more agile longitudinal driving and more

stable cornering (particularly at slippery roads) [2]. Finally, all these benefits can be combined and maximized if four e-motors are used to independently drive each wheel.

For the commanded total longitudinal force (or acceleration) and the demanded yaw torque (zero for straight-line driving), the four e-motor drive vehicle is characterized by two redundant degrees of freedom (DOF). That is, two torque distribution coefficients can be freely allocated to minimize the battery energy consumption, i.e., to maximize the vehicle range [3]. In the cost-effective case of two front/rear-axle e-motors, there is still a single DOF to optimally allocate, i.e., a front/rear axle torque distribution coefficient can be optimized for energy-efficient driving. It is analytically proven in [4] that, for the assumptions of equal e-motors and a specific realistic shape of e-motor power loss vs. torque demand curve (monotonically rising one with a characteristic saddle point), the optimal front/rear torque distribution is such that the single-axle (either front or rear) mode is used for low total torque demand, while the AWD mode with 50:50% torque split is employed for mid-high total torque demand. The torque switching point depends on the vehicle velocity, and it can be determined either numerically [4] or analytically [5]. It is shown in [5] that, when accounting for the longitudinal tire slip loss minimization, the single-axle operation should be assigned to rear axle during acceleration and the front axle for (regenerative) braking. That is, the torque should be transferred to the axle with higher friction potential (due to the varying normal load).

The above energy-efficient torque distribution rule can also be applied in the cornering case, where the four-motor drive is split into left- and right-side tracks [4]. To minimize the lateral tire slip loss, the outer-track motors are first considered, where only a single motor is used at low torque demands (the rear outer one for acceleration and the front outer one for deceleration). If the total torque demand exceeds the first torque switching point, both outer motors are used in the 50:50% split [5]. As the torque demand further grows, first a single and then both inner motors get engaged, i.e., the number of motors continues to be progressively increased to three- and then four-wheel drive configuration. Analytical expressions for the three torque switching points and the related active yaw torque brake points are derived in [5]. The overall rule-based (RB) feedforward torque vectoring strategy is implemented in [6] and connected with a superimposed lateral stability controller. It has been demonstrated in [4-6] that the simple-to-implement RB controller provides the corrected/active vehicle understeer characteristic which is close to the globally optimal understeer characteristic, and which leans toward the neutral steer characteristic for sporty feel, still with some considerable stability reserve.

Since the e-motor (particularly the permanent magnet ones) are prone to idling drag loss, the use of disconnect clutches (typically dog clutches) have been considered in the automotive industry to disconnect the motors that are not active. For instance, the rear motors are disconnected when the front-axle motor(s) are active, thus avoiding the rear motor drag loss and improving the energy efficiency and vehicle range. However, the round-trip energy loss caused by (i) the energy drawn from the battery for the motor startup to synchronize the dog clutch and (ii) the energy recuperated by decelerated motor after the clutch is disconnected should be taken into account in the vehicle model used in optimization and optimal control. This model is dynamic by its nature even if the simple kinematic, backward-looking powertrain description is considered, because the clutch state in the previous sampling step is required to calculate the transient (connect/disconnect) loss in the current step. Next, the dynamic nature of powertrain behavior prevents the instantaneous control allocation from being globally optimal, i.e., the knowledge of forthcoming driving cycle is needed to find the globally optimal e-motor torque control trajectories. The optimization could be subject to

limited clutch disconnect frequency for clutch durability reasons. Finally, for the same reasons the rule-based control strategy should be modified in the presence of disconnect losses, or ultimately a predictive control strategy should be designed.

To the best of authors' knowledge, optimization and optimal control of torque distribution of BEV e-motors with disconnect functionality has barely been investigated in the available literature. A rare exemption is [7] (see also [3]), where a considerable battery energy consumption is reported when employing the disconnect option. However, this reference apparently neglects the disconnect transient loss, i.e., uses the same control allocation techniques as in the case of permanently connected motors [4-6]. To fill the research gap, this paper presents a summary of the authors' recent research work in the field of modeling, control trajectory optimization, rule-based control, and model predictive control of BEV straight-line driving torque vectoring in the presence of clutch disconnect functionality. A more detailed elaboration of the particular developments is presented in [8-10].

The remaining part of this paper is organized into six sections. Section 2 describes a backward-looking four-motor BEV powertrain dynamic model that accounts for e-motor connect/disconnect energy losses. Dynamic programming (DP)-based control trajectory optimization method is presented in Section 3 along with instantaneous optimization results. Section 4 proposes an RB control strategy based on a set of speed-dependent torque switching curves with a hysteresis. The same section presents an ultimate model predictive control (MPC) strategy, which utilizes the DP optimization algorithm developed in Section 3. The developed control strategies have been verified by computer simulations for various certification driving cycles, and the results are compared with the globally optimal DP benchmark, as well as with the baseline control strategies based on even torque distribution and optimal allocation with no disconnect option.

2. MODELING

A direct four-wheel drive case is assumed, where equal e-motors are connected to each wheel via a gear with the speed ratio h and a disconnect dog clutch. The longitudinal vehicle dynamics parameters are adopted from Chevrolet Volt extended range electric vehicle (EREV) [11], with certain adjustments of the vehicle mass m_v and the center of gravity height h_{COG} to account for increased battery mass when applied to the BEV. The smaller of two EREV's permanent magnet synchronous motors is taken as the BEV e-motor. Its power is 55

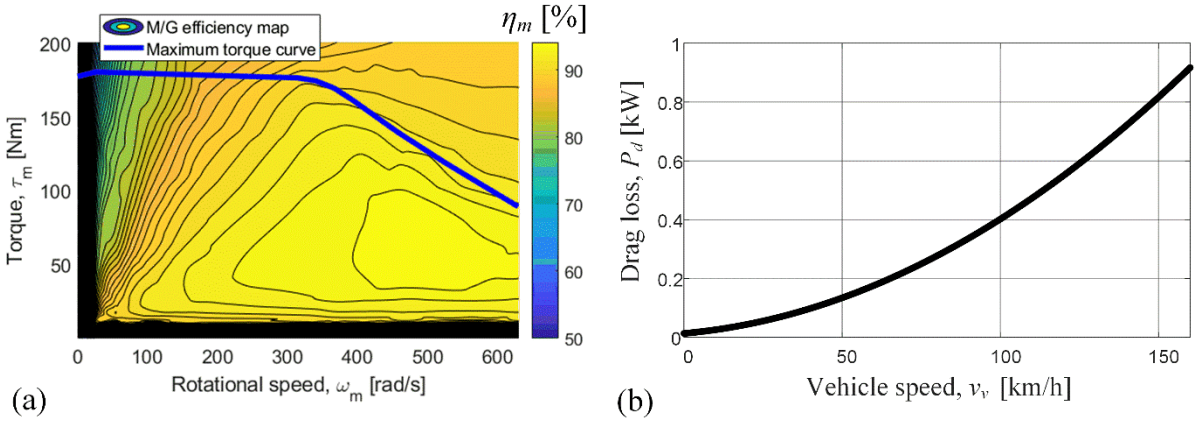

Fig. 1. E-motor efficiency and maximum torque maps (a) and drag loss characteristic (b).

kW, i.e., the total installed BEV power is 220 kW. The e-motor efficiency map and the maximum torque curve are shown in Fig. 1a. The connected, but unselected e-motor (zero torque command) imposes a speed-dependent drag power loss. The drag loss has firstly been estimated based on the extrapolation of power loss curves obtained from the map in Fig. 1a, and then adjusted for a more realistic progressive characteristic in accordance with experimental data from [6]. The obtained drag loss characteristic is shown in Fig. 1b.

The computationally efficient backward-looking vehicle modeling approach is used to facilitate the optimization study [12]. The powertrain variables are calculated in the direction from wheels towards e-motors (so, in the backward manner). The total wheel torque demand is determined from the driving cycle-defined vehicle velocity v_v based on the vehicle longitudinal dynamics equation:

$$\tau_{w,t} = \sum_{i=1}^{4} \tau_{w,i} = (m_v \dot{v}_v + m_v g \sin\alpha + R_o m_v g \cos\alpha + 0.5 \rho_{air} C_d A_f v_v^2) r \tag{1}$$

where α is the road slope (set to zero for certification driving cycles used herein), r is the effective tire radius, g is the gravity acceleration, R_o is the rolling resistance coefficient, ρ_{air} is the air density, C_d is the aerodynamic drag coefficient, A_f is the vehicle frontal area, and $\tau_{w,i}$, i = 1, 2, 3, 4, is the torque of front-left, front-right, rear-left, and rear-right wheel, respectively. For the considered case of straight-line driving, the yaw torque is set to be equal to zero, thus giving

$$\tau_{w,1} - \tau_{w,2} + \tau_{w,3} - \tau_{w,4} = 0 \tag{2}$$

By defining the front-rear torque distribution through the dimension-less coefficient $\sigma = (\tau_{w,1} + \tau_{w,2})/\tau_{w,t}$ and the front- and rear-axle left-right torque distributions through $\rho_f = \tau_{w,1}/(\tau_{w,1} + \tau_{w,2})$ and $\rho_r = \tau_{w,3}/(\tau_{w,3} + \tau_{w,4})$, respectively, and solving Eqs. (1) and (2), one obtains [3]:

$$\begin{aligned} \tau_{w,1} &= \sigma \rho_f \tau_{w,t} \\ \tau_{w,2} &= \sigma(1 - \rho_f)\tau_{w,t} \\ \tau_{w,3} &= (1 - \sigma)\rho_r \tau_{w,t} \\ \tau_{w,4} &= (1 - \sigma)(1 - \rho_r)\tau_{w,t} \end{aligned} \tag{3}$$

with

$$\rho_r = \begin{cases} \dfrac{\sigma\rho_f - 0.5}{\sigma - 1}, & \text{if } \sigma \neq 1, \\ 0.5, & \text{otherwise.} \end{cases} \tag{4}$$

Eqs. (3) are used to calculate the individual wheel torques $\tau_{w,i}$ for the given total torque demand $\tau_{w,t}$ and the control inputs $\sigma \in [0, 1]$ and $\rho_f \in [0, 1]$ commanded by the control strategy.

If **the clutch is connected**, the wheel torque $\tau_{w,i}$ is transformed to the motor torque $\tau_{m,i}$ based on equation

$$\tau_{m,i} = \frac{1}{h}\left(\tau_{w,i}\eta_{tr}^{k_t}(\tau_{w,i}) + \frac{P_0(\omega_{w,i})}{\omega_{w,i}}\right), \tag{5}$$

which takes into account the gearbox efficiency η_{tr} and the transmission idling loss P_0 (described by the maps from [11], adjusted for lower BEV gearbox loss when compared to EREV transmission loss), and where k_t equals -1 for $\tau_{w,i} \geq 0$ (motoring) and 1 for $\tau_{w,i} < 0$ (regenerative braking). The motor speed is determined as

$$\omega_{m,i} = h\omega_{w,i} = h\frac{v_v}{r(1 - s_{x,i})} \tag{6}$$

where $s_{x,i}$ is the longitudinal slip determined from the linearized tire model as

$$s_{x,i} = \frac{\tau_{w,i}}{rk_x(F_{z,i})} \tag{7}$$

where k_x is the tire longitudinal stiffness, whose dependence on the tire normal load F_{zi} is obtained from the LuGre tire friction model [13]. The tire normal load distribution is defined by [3]:

$$\begin{aligned} F_{z1,2} &= \frac{1}{2}m_v\left(\frac{l_r}{l}g - \frac{h_{COG}}{l}\dot{v}_v\right) \\ F_{z3,4} &= \frac{1}{2}m_v\left(\frac{l - l_r}{l}g + \frac{h_{COG}}{l}\dot{v}_v\right) \end{aligned} \tag{8}$$

where l is the distance between front and rear axle, and l_r is the distance between rear axle and COG. The e-drive electric power is given by

$$P_{el,i} = \tau_{m,i}\omega_{m,i} + P_{m,loss,i}(\omega_{m,i}, \tau_{m,i}) \tag{9}$$

where the power loss term reads

$$P_{m,loss,i} = \begin{cases} \omega_{m,i}\tau_{m,i}\left(\eta_{m,i}^{\nu}(|\omega_{m,i}|, |\tau_{m,i}|) - 1\right), & \text{if } \tau_{w,i} \neq 0, \\ P_d(|\omega_{m,i}|) + P_0(\omega_{w,i}), & \text{if } \tau_{w,i} = 0. \end{cases} \tag{10}$$

where ν equals -1 for $\tau_{m,i} \geq 0$ (motoring) and 1 for $\tau_{m,i} < 0$ (regenerative braking).

When the **e-motor is connecting**, it first needs to start up to reach the wheel speed referred to the clutch shaft ($h\omega_{w,i}$). In that moment the dog clutch is synchronized, and it can be locked, which gives $\omega_{m,i} = h\omega_{w,i}$. The synchronization process requires the energy to be drawn from the battery (E_c). This energy has been determined off-line by simulating the e-motor speed control system consisting of a proportional-integral (PI) controller tunned according to symmetrical optimum criterion, speed-dependent torque limit based on the limit curve in Fig. 1a, a first-order lag accounting for the motor torque generation dynamics, and the motor rotational dynamics integral term. The motor startup response for the maximum value of target speed $\omega_{m,R}$ is shown in the left half of Fig. 2a. The synchronization energy E_c has been determined by integrating the motor power $\omega_{m,i}\tau_{m,i}\eta_{m,i}^{\nu}$ (cf. Eq. (10)) over the sampling time interval (set to T_d = 1 s herein) for different target/synchronization speeds $\omega_{m,R}$, and the results are shown in Fig. 2b by red line.

After the **e-motor disconnect** command is issued, the clutch is first opened, and the motor speed reference is set to zero ($\omega_{m,R} = 0$). It is assumed that the motor is, consequently, stopped within a single sampling step by using regenerative braking (see right half of Fig. 2a). The recuperated energy $-E_d > 0$ has been determined by means of simulation of the e-motor speed control system for different starting speeds. The results are shown by blue line in Fig. 2b. Note that the gap between the characteristics $-E_d$ and E_c shown in Fig. 2b corresponds to round-trip losses.

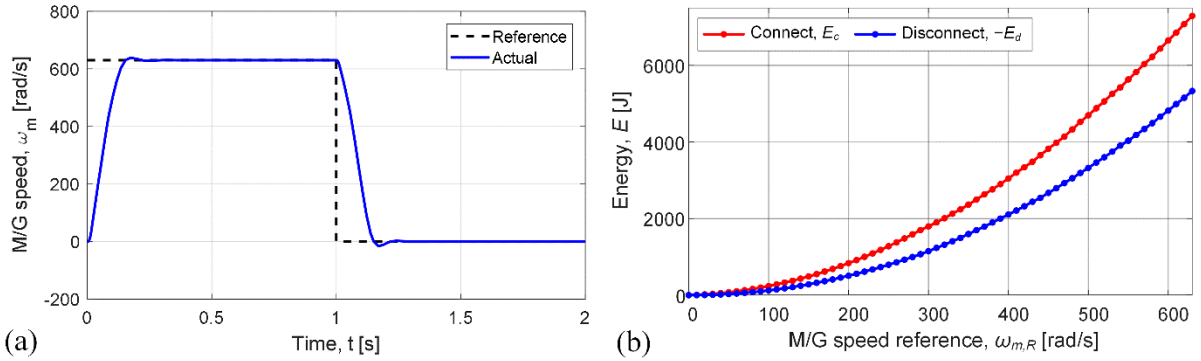

Fig. 2. E-motor speed response during e-motor connecting and disconnecting process for maximum synchronization speed (a) and corresponding values of energy drawn from (E_c) and recharged to battery ($-E_d$) for different synchronization speeds (b).

The **clutch state process** is described by the discrete-time state equation

$$\mathbf{c}(k+1) = [0\ 0\ 0\ 0] \cdot \mathbf{c}(k) + \mathbf{I} \cdot \mathbf{c}_R(k), \tag{11}$$

where $\mathbf{I}$ is the identity matrix, and $\mathbf{c} = [c_1\ c_2\ c_3\ c_4]^T$ and $\mathbf{c}_R(k) = [c_{R,1}\ c_{R,2}\ c_{R,3}\ c_{R,4}]^T$ are the actual and control strategy-commanded (reference) clutch state vectors, respectively, with the clutch state being defined as

$$c_i = \begin{cases} 0, & \text{if clutch is open} \\ 1, & \text{if clutch is locked} \end{cases}, \ i = 1,\ldots,4. \tag{12}$$

The model assumes that the e-motor connect ($c_i(k) = 0$, $c_{R,i}(k) = 1$) and disconnect transient process ($c_i(k) = 1$, $c_{R,i}(k) = 0$) is completed within a single sampling time, i.e., $c_i(k+1) = c_{Ri}(k)$ is valid. According to Fig. 2, it is clear that the transient process completes in 250 ms in the worst case of maximum reference speed step, thus meaning that the above assumption is satisfied for the considered sampling time $T_d = 1$ s, or even for four times smaller sampling time ($T_d = 0.25$ s) that may be more realistic for sporty, AWD BEV. During the whole clutch transient sampling step, the torque is assumed not to be transferred to the corresponding wheel.

Finally, the energy consumed from the battery by the i^{th} e-drive at any sampling instant k is determined as

$$E_{el,i}(k) = c_i(k)c_{R,i}(k)T_d P_{el,i}(k) + \bar{c}_i(k)c_{R,i}(k)E_{c,i}(k) + c_i(k)\bar{c}_{R,i}(k)E_{d,i}(k), \tag{13}$$

where $\bar{x}$ denotes the complement of x (i.e., $\bar{x} = 1$, for $x = 0$, and vice versa).

3. OPTIMIZATION

3.1. Instantaneous optimization

If **no disconnect option** is considered ($c_i(k) = c_{R,i}(k) = 1, \forall i, \forall k$), the vehicle model from Section 2 becomes static (no state equation (11) appears) and the optimal control problem reduces to instantaneous optimization, i.e., optimal control allocation. The optimal control allocation maps can be found off-line in dependence on total wheel torque demand $\tau_{w,t}$ and the vehicle velocity v_v. Fig. 3a shows the optimized map of front-rear torque distribution control input σ for the equal left-right distributions ($\rho_f = \rho_r = 0.5$; see Eq. (3)). Evidently, the optimal solution is such that the σ is either close to 0.5 (AWD with equal front/rear distribution), 0 (RWD), or 1 (FWD). The AWD mode is used above the speed-dependent torque switching curve (red line in Fig. 3a), while the 2WD modes are optimal below this switching curve. The black line in Fig. 3a, which separates the RWD and FWD modes is aligned well with the road load curve (obtained from (1) for $\dot{v}_v = 0$ and $\alpha = 0$). Hence, the RWD mode is optimal for accelerating vehicle ($\dot{v}_v > 0$), while the FWD mode should be used in the case of deceleration ($\dot{v}_v < 0$). Namely, the torque should be transferred to the tires with higher normal load (cf. Eq. (8)), i.e., larger friction circle, which is to minimize the longitudinal tire slip loss. The above findings are in accordance with numerical and analytical results from [3-5].

In the case of uneven left-right torque distribution ($\rho_f \neq 0.5$, $\rho_r \neq 0.5$), i.e., for diagonal or warp torque transfer, on one side of the vehicle the torque would be transferred to a wheel with smaller friction circle. This results in higher energy consumption (i.e., suboptimal behavior) when compared to the nominal case $\rho_f = \rho_r = 0.5$ (see [8] for numerical results).

Fig. 3b shows the optimal control allocation results in the **case of disconnecting e-motors** on the rear axle for $\sigma = 1$ and the front axle for $\sigma = 0$. The results are qualitatively the same as in the case of no disconnect considered (cf. Fig. 3a). However, the AWD-2WD boundary curve (cyan line) is shifted up in Fig. 3b when compared to Fig. 3a. Namely, the 2WD model is

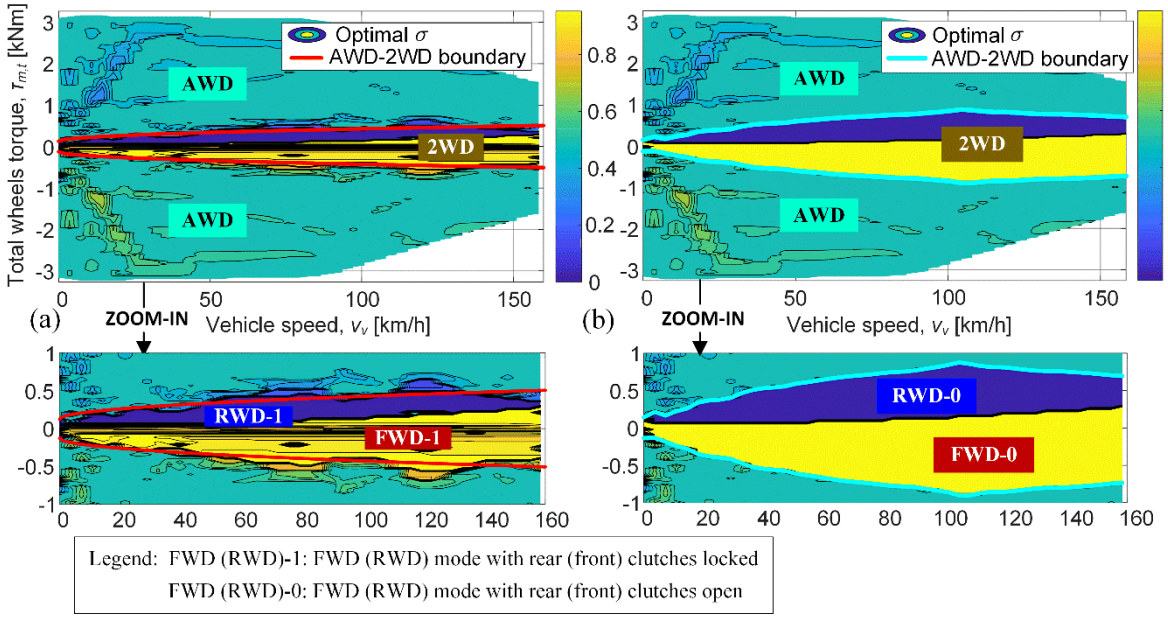

Fig. 3. Instantaneous optimization results when disregarding (a) and accounting for disconnect clutch functionality (b).

active in a wider torque range, which is because the drag loss is absent on the opposite (inactive) axle. Of course, there are transient losses when switching from 2WD to AWD mode and vice versa, which are disregarded in Fig. 3b. They can only be taken into account through global optimization based on the dynamic vehicle model (see next subsection).

3.2. Control trajectory optimization

When considering the disconnect clutch functionality, including the corresponding switching losses, the full dynamic model from Section 2 should be used. The optimization problem is then defined through time, i.e., the trajectories of control variables $\sigma(k)$ and $\mathbf{c}_R(k)$ are optimized over the whole driving cycle (herein, ρ_f is set to 0.5 according to discussion in Subsection 3.1; see [8] for more general consideration). The cost function to be minimized is defined as

$$J = \sum_{k=0}^{N_f-1} \left(F_{sw}(k) + \sum_{i=1}^{4} E_{el,i}(k) \right), \tag{14}$$

where the e-drive energy consumption $E_{el,i}$ at each sampling step k is defined by Eq. (13), and $N_f = t_f / T_d$ is the number of sampling steps of a driving cycle of length t_f. The term $F_{sw}(k)$ penalizes frequent clutch switching to avoid clutch durability issues, and it is defined as

$$F_{sw}(k) = \begin{cases} 0, & \text{if } \mathbf{c}_R(k) = \mathbf{c}(k), \\ K_{sw}, & \text{otherwise}, \end{cases} \tag{15}$$

where K_{sw} is the switching penalization coefficients, which is set as a trade-off between energy efficiency and durability.

The optimization is subject to process dynamics defined by the state equation (11) and a set of nonlinear algebraic equations presented in Section 2, where it is assumed that the clutches are initially locked. It is also formally requested that the clutches are locked at the end of driving cycle, i.e., that the final condition corresponds to the initial condition for sustaining operation over multiple driving cycles:

$$\mathbf{c}_i = \mathbf{c}(0) = \mathbf{c}_f = \mathbf{c}(N_f) = [1\ 1\ 1\ 1]^{\mathrm{T}}. \tag{16}$$

The inequality constraints include those on maximum motor torque (see Fig. 1a) and maximum tire force:

$$-\tau_{m,\max}(|\omega_{m,i}|) < \tau_{m,i} < \tau_{m,\max}(|\omega_{m,i}|), \tag{17a}$$

$$-\mu F_{z,i} < \tau_{w,i}/r < \mu F_{z,i}, \tag{17b}$$

where μ is the tire-road friction coefficient and $F_{z,i}$ is the tire normal load given by Eq. (8). Also, to avoid drivetrain torque interruption, commanding clutch disconnect is allowed only on a single axle, providing that the clutches on opposite axle are connected:

$$\mathbf{c}_R(k) \in \begin{cases} \{[1\ 1\ 0\ 0]^{\mathrm{T}}, [1\ 1\ 1\ 1]^{\mathrm{T}}\}, & \text{if } \mathbf{c}(k) = [1\ 1\ 0\ 0]^{\mathrm{T}}, \\ \{[0\ 0\ 1\ 1]^{\mathrm{T}}, [1\ 1\ 1\ 1]^{\mathrm{T}}\}, & \text{if } \mathbf{c}(k) = [0\ 0\ 1\ 1]^{\mathrm{T}}, \\ \{[1\ 1\ 0\ 0]^{\mathrm{T}}, [0\ 0\ 1\ 1]^{\mathrm{T}}, [1\ 1\ 1\ 1]^{\mathrm{T}}\}, & \text{if } \mathbf{c}(k) = [1\ 1\ 1\ 1]^{\mathrm{T}}. \end{cases} \tag{18}$$

The optimization is based on the dynamic programming (DP) algorithm [11] because it can provide a globally optimal solution for the particular case of nonlinear and discontinuous

system. The main weakness of the DP algorithm is that it is computationally demanding and, thus, applicable to systems of a low dimensionality. This is the case here owing to the use of backward vehicle model, and the fact that clutch state and control inputs $\mathbf{c}$ and $\boldsymbol{c}_R$ are binary variables (i.e., quantized in only two levels). Based on the instantaneous optimization results from Subsection 3.1, even the front-rear torque distribution control input σ can be quantized in a couple of levels (e.g., 0, 0.5, and 1; see Section 6) for enhanced computational efficiency. Note, that by quantizing the states and control inputs, their limits are automatically imposed, so that there is no need for additional inequality constraints.

The DP algorithm is executed off-line in two phases. Firstly, starting from the final condition $\mathbf{c}_f$ and accounting for the discrete-time system state-space model and the inequality constraints (17) implemented as soft constraints (additive to cost function), the control input vector [σ; $\mathbf{c}_R$] is found in the time step N_f-1 to minimize the cost function contribution in the final step of driving cycle for all values of state vector $\mathbf{c}$ in the time step N_f-1. The optimized control vectors are stored in memory, and the optimization process is repeated recursively backward in time. Started from the known initial state vector $\mathbf{c}(0)$, the corresponding optimal control vector in the 0^{th} step is selected, which is then employed together with the system model to calculate the next state vector $\mathbf{c}(1)$ and corresponding optimal input vector, and the calculation is continued forward in time until the whole control vector is retrieved. Non-allowed combinations of $\mathbf{c}(k)$ and $\mathbf{c}_R(k)$, according to Eq. (18), are not considered as the optimal candidates. More details on the DP algorithm realization are provided in [8].

4. CONTROL

4.1. Rule-based control

The rule-based (RB) strategy is originally motivated by the instantaneous optimization results shown in Fig. 3, which are summarized through the boundary curves replotted in Fig. 4. Since the disconnect clutch functionality is considered herein, the corresponding boundary curve $\tau_{b,d}$ is most relevant for the rule-based strategy. However, because the optimization resulting in this curve does not take into account the e-drive switching losses (Section 3), it may be suboptimal for dynamic driving conditions that typically occur in low vehicle velocity range (e.g., city driving). More importantly, implementing this boundary curve in the low-velocity conditions, the clutch disconnects would be frequent, thus affecting the clutch durability. Therefore, clutch disconnect should be avoided in the low-velocity range by using the second boundary line ($\tau_{b,c}$ in Fig. 4), which is obtained through optimization under the assumptions of connected motors (locked clutches). In the region below the line $\tau_{b,c}$, a 2WD mode is active with no clutch disconnect on the opposite axle, so that when a transition to AWD occurs (for the operating point above the line $\tau_{b,c}$), there is no clutch switching.

In the mid-high velocity range, a smooth transition from the no-disconnect optimal line $\tau_{b,c}$ to the disconnect optimal line $\tau_{b,d}$ should be provided. This is realized through exponential function (see green line in Fig. 4):

$$\tau_{b,d}^{*}(v_v) = \tau_{b,d}(v_v)\left(1 - e^{-\frac{v_v - \Delta v_v}{V_c}}\right), \tag{19}$$

whose origin is defined by the velocity shift parameter Δv_v, and which converges to the optimized line $\tau_{b,d}$ for the velocities $v_v > \Delta v_v + 3V_c$ (tunable via the velocity constant parameter V_c). Note that only the upper boundary lines $\tau_{b,d}$ and $\tau_{b,c}$ are labeled in Fig. 4, and $\tau_{b,d}$ is used to calculate $\tau_{b,d}^{*}$ according to (19). The lower boundary lines need to be mapped,

as well, and used to calculate the lower boundary counterpart of $\tau_{b,d}^{*}$ (all shown in Fig. 4), where the parameters Δv_v and V_c remains the same as in the case of upper line.

Finally, to further suppress the clutch disconnects and make the results closer to the DP benchmark [9], a hysteresis is introduced to the disconnect line $\tau_{b,d}^{*}$ (see magenta line in Fig. 4). The upper part of the hysteresis-related dashed line is described as (cf. (19)):

$$\tau_{b,dh}^{*}(v_v) = K_h \tau_{b,d}(v_v)\left(1 - e^{-\frac{v_v - \Delta v_v - \Delta v_{vh}}{V_c}}\right), \tag{20}$$

where the hysteresis is defined by the downscaling gain $0 < K_h < 1$ and the horizontal shift $\Delta v_{vh} > 0$.

As described in Section 3 and designated in Fig. 3, when operating in the 2WD mode (below red and green lines in Fig. 4), the optimal solution is such that RWD is used above the road load line (brown line), and the FWD is active below this line. Such a law would make the control strategy more complex (particularly from the standpoint of forbidding the direct FWD/RWD transitions when disconnect is active; see the constraint (18)) and would increase the frequency of clutch switching (occurs for all motors at the transition over the brown line in the region below green line). On the other hand, the DP results from [8] point out that the energy savings when using both FWD and RWD rather than either FWD or RWD are negligible (a fraction of percent for the given vehicle and test scenarios), which is explained by a negligible influence of the longitudinal tire slip loss when compared to the e-drive loss [5]. Hence, the proposed RB strategy relies on RWD mode only when the 2WD mode is active (FWD mode could be used instead, with a marginal influence on results, [8]).

The final RB control strategy is, thus, defined by the red, green, and magenta boundary lines, which define four characteristic modes of operation (Fig. 4):

1) RWD with the front-axle motors connected (**RWD-1**, between red and green lines),
2) **AWD** (beyond red and green lines),
3) RWD with the front-axle motors disconnected (**RWD-0**, within magenta lines), and
4) Keeping previous clutch states $\mathbf{c}(k-1)$ (between green and magenta lines); more specifically, mode(k) is set to: RWD-0 if $\mathbf{c}(k-1) = [0\ 0\ 1\ 1]^{\mathrm{T}}$, AWD if $\mathbf{c}(k-1) = [1\ 1\ 1\ 1]^{\mathrm{T}}$ and the operating point lies beyond the (expanded) red lines, and RWD-1, otherwise.

Accordingly, the clutch control input is defined as

$$\mathbf{c}_R(k) = \begin{cases} [0\ 0\ 1\ 1]^{\mathrm{T}}, & \text{if RWD-0,} \\ [1\ 1\ 1\ 1]^{\mathrm{T}}, & \text{if RWD-1 or AWD,} \end{cases} \tag{21}$$

while the front-rear torque distribution coefficient σ is set according to the following rule (see Section 3):

$$\sigma(k) = \begin{cases} 0, & \text{if RWD-0 or RWD-1,} \\ 0.5, & \text{otherwise.} \end{cases} \tag{22}$$

The RB strategy has four free parameters (Δv_v, V_c, K_h, and Δv_{vh}), which should be optimized for the best performance. The parameter optimization procedure has been performed in three characteristic steps (see [9] for details): (i) preparing the sets of discrete values for all the four

parameters; (ii) iterating through all parameter combinations, performing vehicle simulation for a given driving cycle, and saving the values of energy consumption and number of clutch state changes; (iii) performing Pareto filtering of the saved results (in the two criteria) to obtain a Pareto frontier, which can be compared with the DP benchmark frontier obtained for different values of weighting coefficient K_{sw} (Section 5).

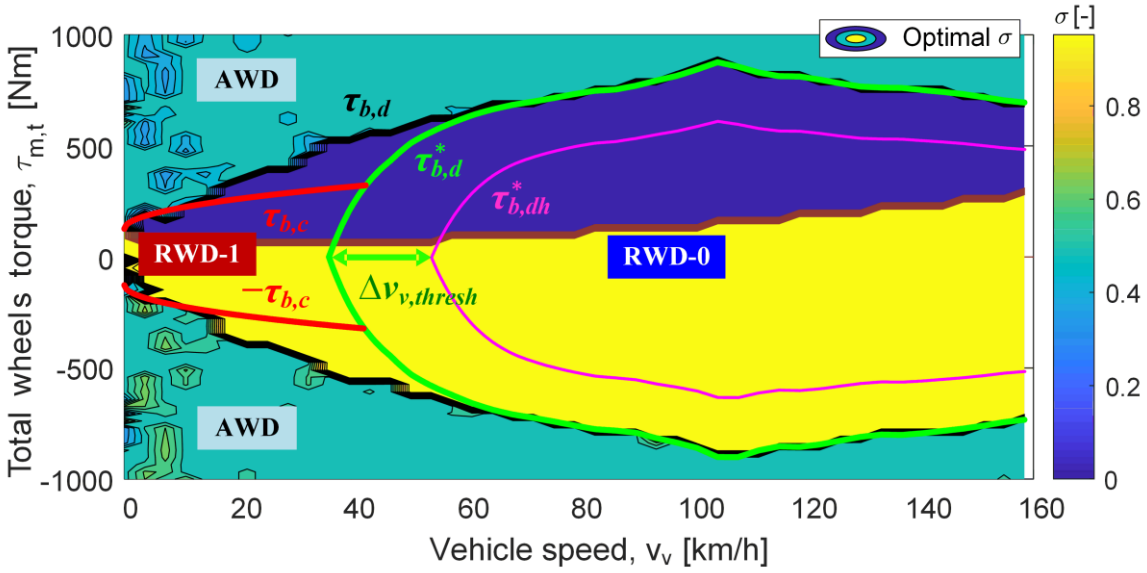

Fig. 4. Boundary curves of RB control strategy.

4.2. Model predictive control

The DP algorithm assumes the full knowledge of driving cycles, and it is aimed for off-line control trajectory optimization. When applied on a receding horizon of N_p steps, it becomes a part of on-line-executable model predictive control (MPC) strategy. The DP optimization is applied at any sampling step k on the receding horizon $[k, k+N_p-1]$, thus giving the optimal control trajectories $\sigma(k)$ and $c_R(k)$. The first sample of those control inputs is applied in the sampling step k. The calculation process is then repeated in every next sampling step.

The DP algorithm remains as described in Section 4, with the following exceptions: (i) the final condition of (16) is disregarded, as it cannot be implemented in a straightforward way and has a minor practical meaning (the vehicle velocity is zero at the end of driving cycle/trip, and the clutches can readily be locked immediately after the trip), (ii) the forward phase is omitted as only the first control input is needed (i.e., applied), and (iii) the control input σ is quantized in a couple of (nearly-optimal) levels (here, 0, 0.5, and 1) with a negligible influence on accuracy (see discussion in Section 5 and [8]).

To perform the DP optimization on the prediction horizon, the vehicle (city bus) velocity should be known/predicted for that portion of trip. The velocity prediction is typically performed by using neural network (NN) models. It is shown in [14] that the NN prediction accuracy can be high for the length of prediction horizon of up to $N_p \cong 10$ steps, and that this can provide effective DP-based MPC of a plug-in hybrid electric vehicle (PHEV). The same should be valid for BEV torque vectoring MPC, as an expectedly less complex control problem.

5. RESULTS

Table 1 shows the comparative battery energy consumption results for three control scenarios and various certification driving cycles. The first two rows of the table correspond to the case of no motor disconnect option considered. When compared with the crude strategy based on equal torque distribution (σ = 0.5), the optimal control allocation results in reduction of energy consumption of up to 5%. This is in an agreement with the results published in [1, 3, 4]. In the case of considering the disconnect clutch and applying the proposed DP-based optimization approach (with K_{sw} = 0), the energy consumption is reduced by up to 7% when compared to the optimal allocation approach.

Blue line in Fig. 5 shows the DP optimal results obtained for UDDS driving cycle and the discrete torque split values $\sigma \in \{0, 0.5, 1\}$ used for better computational efficiency of the DP algorithm. The DP results are given in the form of Pareto frontier obtained by varying the weighting factor K_{sw} of the cost function given by (14) and (15). The rightmost point corresponds to no switching frequency penalization (K_{sw} = 0), i.e., minimum energy consumption that equals 1.1241 kWh. This is only 0.05% higher than the corresponding value from Table 1, which is obtained for fine control input discretization $\sigma \in \{0, 0.01, \dots, 1\}$. This confirms that the nearly optimal control allocation values $\sigma \in \{0, 0.5, 1\}$ (Section 3) are nearly optimal in the DP case, as well. The leftmost point of the Pareto frontier in Fig. 5 corresponds to the case of the weighting coefficient K_{sw} being high enough for resulting in no disconnects. The corresponding energy increase of 6.4% correlates with the energy reduction value of 5.8% from Table 1. As a good trade-off between the energy efficiency and durability, the designer may opt for a Pareto optimal point placed at the knee of frontier, e.g., the one corresponding to 20 clutch state changes (per the length of the UDDS cycle of 1370 s or 11.99 km) and 0.63% of energy consumption increase when compared to the rightmost, minimum energy point.

Fig. 5 also shows the Pareto optimal results obtained by applying the proposed RB control strategy. The simple-to-implement on-line RB strategy with the hysteresis included (Fig. 4) can approach the off-line DP benchmark by the margin which is widely lower than 1%, and around 2% for the number of clutch changes in the range from 5 to 15. This error margin is even lower for other driving cycles from Table 1 [9]. Inclusion of hysteresis, i.e., memory in the control law, gives consistent and significant energy consumption reduction (cf. green and black lines in Fig. 5).

Fig. 6 shows the MPC strategy verification results for the case of ideal vehicle velocity prediction. In the case of low penalization coefficient K_{sw}, i.e., when allowing for a relatively large number of clutch state change (larger than 40), the performance of MPC strategy approaches the globally optimal DP performance even for short prediction horizons N_p of around 5 steps. When increasing K_{sw} to reduce the number of clutch state changes to around 20, the prediction horizon should be expanded to around 20 steps for the performance to remain close to the DP benchmark. For very high K_{sw} corresponding to a couple of clutch changes, even the RB strategy is very close to the DP benchmark (see also Fig. 5). This is just because the control allocation is optimal when no disconnect option is used.

Table 1. Comparative values of battery energy consumption for different control scenarios and various driving cycles.

Analysis of total energy consumption, $E_{el,t}$ [kWh]							
Disconnect option	**Method**	**Allowed σ**	**Driving cycle**				
			WLTP (α = 0°)	**UDDS (α = 0°)**	**US06 (α = 0°)**	**HWFET (α = 0°)**	**NEDC (α = 0°)**
NO	Even distribution	0.5	3.1679 (+2.6%)	1.2368 (+3.7%)	2.1141 (+1.9%)	2.2477 (+4.2%)	1.3304 (+5.1%)
NO	Control allocation	{0, 0.01, …, 1}	3.0876 (0%)	1.1929 (0%)	2.0753 (0%)	2.1578 (0%)	1.2660 (0%)
YES	Dynamic programming	{0, 0.01, …, 1}	2.9238 (−5.3%)	1.1236 (−5.8%)	1.9762 (−4.8%)	2.0149 (−6.6%)	1.1879 (−6.2%)

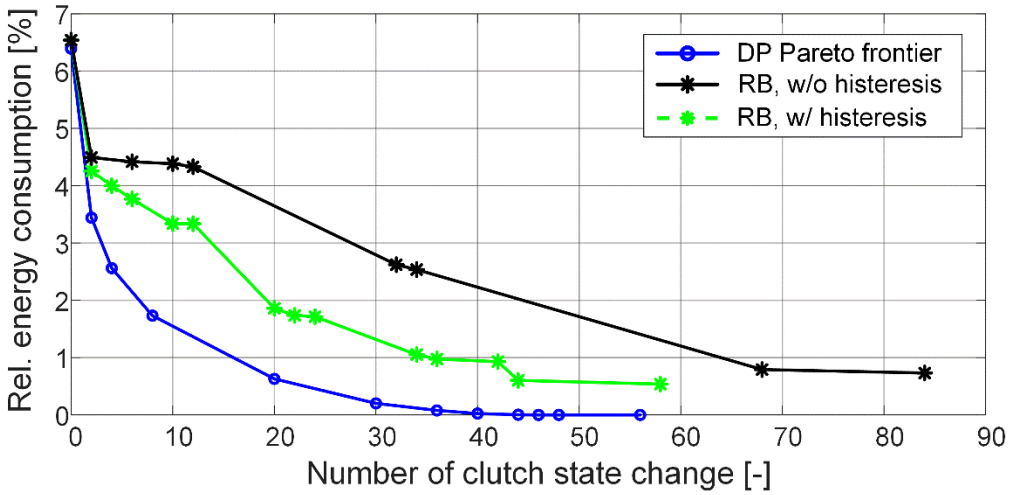

Fig. 5. Pareto frontiers obtained by off-line DP control trajectory optimization and on-line RB control strategy without and with hysteresis (UDDS driving cycle).

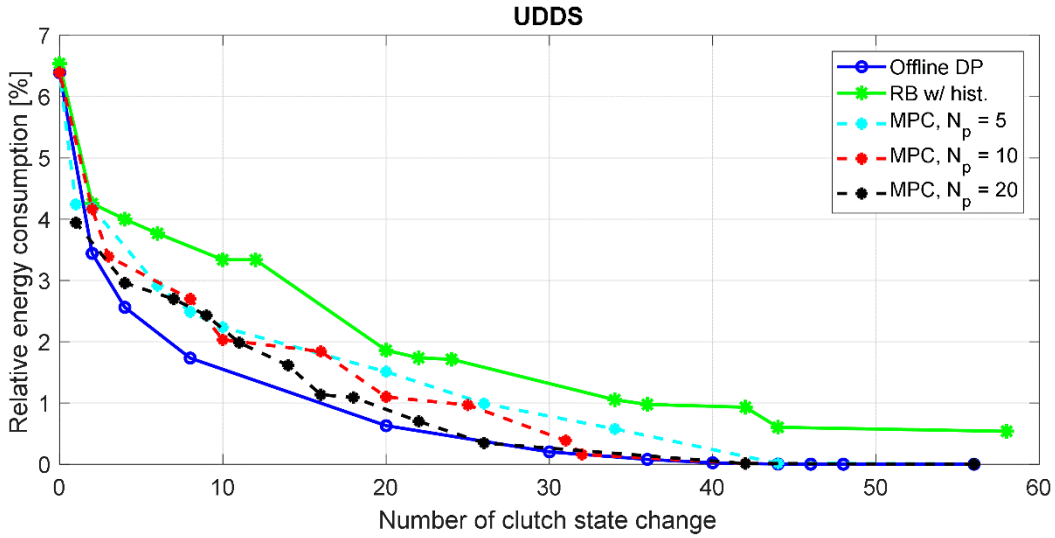

Fig. 6. Pareto frontiers obtained by MPC strategy for different prediction horizon lengths and shown along RB and DP frontiers (UDDS driving cycle).

6. CONCLUSION

The dynamic programming (DP)-based control trajectory optimization results have indicated that introducing the disconnect clutch reduces the multiple-motor electric vehicle energy consumption by around 6% for various certification driving cycles, which is on top of up to 5% reduction achieved by torque distribution itself. The parameter-optimized rule-based (RB) and model predictive control (MPC) strategies approach the DP energy consumption benchmark within the margin of 1.3% and 0.6%, respectively. Having in mind the complexity of the MPC strategy and the fact that the test results do not reflect velocity prediction errors, the RB control strategy is deemed to be more suitable for applications.

More detailed analyses including those related to validation of backward-looking versus forward-looking vehicle model, robustness of RB strategy and its evaluation for a higher share of transient losses, influence of sampling time reduction towards the clutch synchronization time of around 250 ms, sensitivity of MPC strategy to velocity prediction errors and length of prediction horizon, and more comprehensive simulation verification are presented in the individual publications [8-10].

ACKNOWLEDGMENT

It is gratefully acknowledged that this work has been supported by Ford Motor Company.

REFERENCES

[1] P. Gruber, A. Sorniotti, B. Lenzo, G. De Filippis, and S. Fallah, "Energy efficient torque vectoring control", *13th International Symposium on Advanced Vehicle Control* (AVEC '16), Munich, Germany, 2016.

[2] S. De Pinto, P. Camocardi, C. Chatzikomis, A. Sorniotti, F. Bottiglione, G. Mantriota, P. Perlo, "On the Comparison of 2- and 4-Wheel-Drive Electric Vehicle Layouts with Central Motors and Single- and 2-Speed Transmission Systems", *Energies*, Vol. 13, No. 13, 2020.

[3] S. Koehler, A. Viehl, O. Bringmann, and W. Rosenstiel, "Energy-Efficiency Optimization of Torque Vectoring Control for Battery Electric Vehicles", *IEEE Intelligent Transportation Systems Magazine*, Vol. 9, No. 3, pp. 59-74, 2017.

[4] A. M. Dizqah, B. Lenzo, A. Sorniotti, P. Gruber, S. Fallah, and J. De Smet, "A Fast and Parametric Torque Distribution Strategy for Four-Wheel-Drive Energy-Efficient Electric Vehicles", *IEEE Transactions on Industrial Electronics*, Vol. 63, No. 7, pp. 4367-4376, 2016.

[5] G. De Filippis, B. Lenzo, A. Sorniotti, P. Gruber, and W. De Nijs, "Energy-Efficient Torque Vectoring Control of Electric Vehicles with Multiple Drivetrains", *IEEE Transactions on Vehicular Technology*, Vol. 67, No. 6, pp. 4702-4715, 2018.

[6] C. Chatzikomis, M. Zanchetta, P. Gruber, A. Sorniotti, B. Modic, T. Motaln, L. Blagotinsek, and G. Gotovac, "An energy-efficient torque-vectoring algorithm for electric vehicles with multiple motors", *Mechanical Systems and Signal Processing*, Vol. 128, pp. 655-673, 2019.

[7] J. Torinsson, M. Jonasson, D. Yang, and B. Jacobson, "Energy reduction by power loss minimisation through wheel torque allocation in electric vehicles: a simulation-based approach", *Vehicle System Dynamics*, Vol. 60, No. 5, pp. 1488-1511, 2022.

[8] B. Škugor, J. Deur, W. Chen, Y. Zhang, E. Dai, "Backward-looking Modeling and Torque Vectoring Optimization for a Straight-line-driven Electric Vehicle with Four Motors and Disconnect Clutches", *in submission for a journal publication*.

[9] B. Škugor, J. Deur, W. Chen, Y. Zhang, E. Dai, "A Parameter-optimized Rule-based Control Strategy for Front-rear Torque Vectoring in Electric Vehicles with Multiple Motors and Disconnect Clutches", *in submission for a journal publication*.

[10] B. Škugor, J. Deur, W. Chen, Y. Zhang, E. Dai, "A Model Predictive Control Strategy for Front-rear Torque Vectoring in Electric Vehicles with Multiple Motors and Disconnect Clutches", *in submission*.

[11] J. Deur, M. Cipek, B. Škugor, J. Petrić, "Modeling and Low-level Control of Range Extended Electric Vehicle Dynamics", *International Conference on Powertrain Modeling and Control* (PMC 2012), Bradford, UK, 2012.

[12] L. Guzzella, A. Sciaretta, *Vehicle Propulsion Systems*, 2nd ed., Springer Verlag, Berlin, 2007.

[13] J. Deur, J. Asgari, D. Hrovat, "A 3D Brush-type Dynamic Tire Friction Model", *Vehicle System Dynamics*, Vol. 42, No. 3, pp. 133-173, 2004.

[14] J. Soldo, B. Škugor, J. Deur, "Model Predictive Control of a Parallel Plug-in Hybrid Electric Vehicle Relying on Dynamic Programming and Extended Backward-looking Model", *IEEE Transactions on Control Systems Technology*, in review.